ANNALS OF GEOPHYSICS, 68, 2, DM216, 2025; doi:10.4401/ag-9229
OPEN ACCESS

Investigation of Potential Structures in the Southeastern Aegean Region Using Seismological and Gravity Data

Burçin Didem Tamtaş[*,1] and Hazel Deniz Toktay[1]

(1) Istanbul University-Cerrahpasa, Faculty of Engineering, Department of Geophysical Engineering, Buyukcekmece Campus, Istanbul, 34500, Turkey

Article history: received December 19, 2024; accepted Mach 31, 2025

Abstract

This study investigates potential structure distribution in the southeastern Aegean Region, a seismically active and complex region of the Eastern Mediterranean. Using gravity data from the TOPEX v29.1 database, the Fast Sigmoid (FSED) and Tilt Angle of the Horizontal Gradient (TAHG) methods were applied to detect potential structural boundaries. Earthquake and focal mechanism catalogs compiled from various databases were also used to interpret the identified structural edges. A total of 69 structure boundaries were detected, some of which are potential faults related to existing faults. The results of this study provide new insights into the region's tectonic framework, revealing both the continuity of known faults and the identification of new potential faults, thus contributing valuable information on the region's seismotectonic characteristics.

Keywords: Edge detection; Fast Sigmoid; Gravity data; Seismotectonics; Southeastern Aegean Region; Tilt Angle of the Horizontal Gradient

1. Introduction

The southern Aegean Sea, which hosts the Hellenic subduction zone, stands out as one of Europe's most seismically active complex seismotectonic regions and is the subject of geoscientific investigations for the understanding of the current seismotectonic of the Aegean (Andinisari et al., 2020; Friederich et al., 2013; Kiratzi, 2014; Kiratzi and Louvari, 2003; Kkallas et al., 2013; Kuleli, 1997; Main and Burton, 1989; Papadopoulos et al., 1986; Papazachos et al., 1998; Papazachos, 1999; Tan, 2013; Vamvakaris et al., 2016). Inhabited for millennia, the Turkish and Greek coastlines bear witness to the enduring impact of this seismic activity, including historically devastating tsunamis (Altınok and Ersoy, 2000; Ambraseys and Synolakis, 2010; Di Maro and Maramai, 1992; Dominey-Howes, 2002; Dominey-Howes et al., 2000; Galanopoulos, 1960; Karkani et al., 2021; Papadopoulos and Chalkis, 1984; Papadopoulos et al., 2014; Triantafyllou and Papadopoulos, 2024; Triantafyllou et al., 2020). Two major tectonic movements control the region's tectonic activity: the subduction of the African lithospheric plate beneath the Aegean and the movement of the Anatolian Plate to the west and the counterclockwise rotation to the southwest. According to satellite geodesy models, the African Plate is moving in a northerly direction

relative to Eurasia at a rate of about 10 mm/yr, shaping the Hellenic subduction zone (McClusky et al., 2000; Reilinger et al., 2006) (Fig. 1). The Anatolian plate moves to the southwest at 30-40 mm/yr, causing extension in the Aegean area (Jackson et al., 1994; Le Pichon and Angelier, 1979; Le Pichon and Angelier, 1981; McClusky et al., 2000; McClusky et al., 2003; McKenzie, 1978; Oral et al., 1995; Taymaz et al., 1991; Taymaz et al., 1990). In contrast, seismological and geological investigations reveal that although a compressional stress field does not characterize the westward movement of the Anatolian plate in the Aegean area, it is predominantly under an N-S extensional stress regime (McKenzie, 1972, 1978; McKenzie, 1970; Papazachos et al., 1998; Reilinger et al., 2010). This distinction is essential for understanding the different influences on the tectonic behavior of the region. Normal faulting regimes extending in N-S directions are listed in historical earthquake catalogs (Dimova and Raykova, 2018). Many authors have mentioned the existence of E-W trending faults in the region exhibiting right-lateral or left-lateral components by N-S extension (Dewey and Şengör, 1979; Dogan et al., 2021; Emre et al., 2011; Eyidoğan, 2022; Jackson et al., 1994; Jackson and McKenzie, 1988; Papazachos et al., 1998; Tan et al., 2014; Taymaz et al., 1991; Tepe and Sözbilir, 2017).

The reason for the N-S directed extension in the Aegean region is the slab pull force in the Mediterranean (Brun et al., 2017; Doglioni et al., 2002; Kahveci et al., 2019; Le Pichon, 1983; Le Pichon and Angelier, 1979; Mercier et al., 1989; Seyitoğlu and Scott, 1996; Sorel et al., 1988; Sternai et al., 2014). The region has many faults with different characteristics and lengths. Many earthquakes in the Aegean Sea are normal faulting with right-lateral strike-slip components (Taymaz et al., 1991).

Active normal faults extending in E-W, NE-SW and NW-SE directions and strike-slip faults developing between these normal faults are the product of tectonic expansion movements in the NE-SW direction that are dominant throughout the entire Aegean (Eyidoğan, 2022). Detecting faults in an area and determining the focal mechanisms of earthquakes occurring on these faults clarify the tectonic setting. It also provides information about the stress field orientations. The focal mechanisms of earthquakes in the broader Aegean Sea area have been determined via several investigations (Baker et al., 1997; Cambaz and Mutlu, 2016; Delibasis, 1968; Friederich et al., 2013; Hatzfeld et al., 1997; Hatzfeld et al., 1996; Hatzfeld et al., 1989; Hodgson and Cock, 1957s; Kiratzi, 2014; Kiratzi

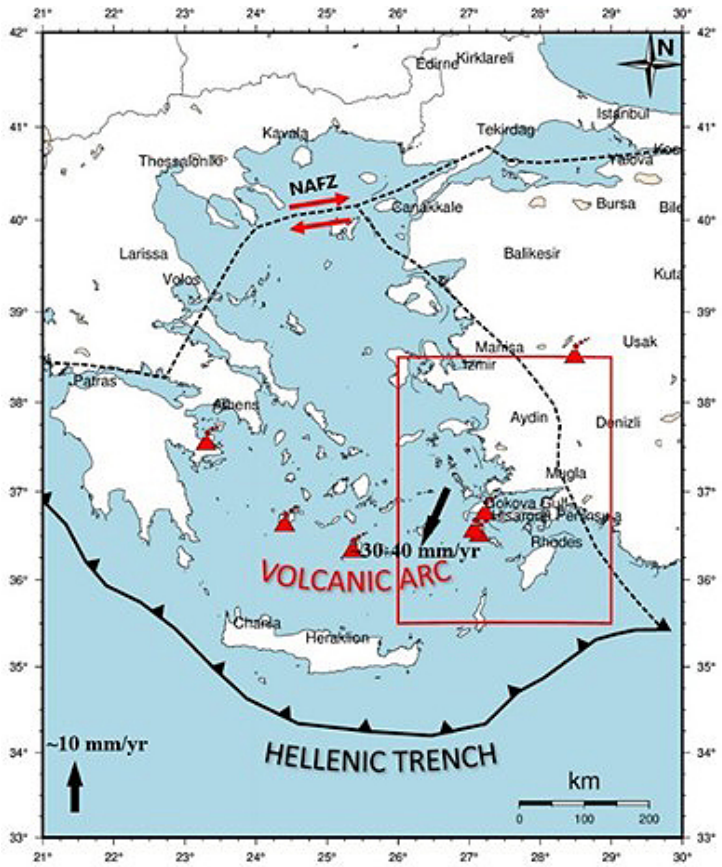

Figure 1. The geodynamic and tectonic structures of the broader Aegean region (NAFZ: North Anatolian Fault Zone).

and Louvari, 2003; Kiratzi and Langston, 1989, 1991; Kiratzi et al., 1991; McKenzie, 1972, 1978; Moshou, 2020; Papadimitriou, 1993; Papazachos 1961; Papazachos et al., 1998; Paradisopoulou et al., 2006; Ritsema, 1974; Roumelioti et al., 2011; Taymaz et al., 1991; Taymaz et al., 1990).

Geological mapping of a specific region, as well as applications in environmental and engineering fields, often requires the interpretation of potential field data in terms of edge detection to outline the horizontal boundaries of the underlying features (Fedi and Florio, 2001; Hsu et al., 1996). Gravity maps are often used to delineate geological contacts and faults. Over the years, several edge detections filters have been developed and improved to obtain better solutions for detecting edges of geological structures from potential field data, including the first order vertical derivative (VDR or FVD), analytic signal (ASA), tilt angle (TA), total horizontal derivative (THDR), theta map (TM), and hyperbolic tilt angle (HTA). The edge detection filters are mostly based on horizontal and vertical derivatives of the field (Alvandi and Ardestani, 2023). On the other hand, edge detection approaches that rely solely on gradient amplitude have demonstrated considerable shortcomings in identifying both shallow and deep anomalous discontinuities (Alvandi and Ardestani, 2023). Researchers have, therefore, designed phase-based filters to determine the lateral boundaries of potential sources (Ai et al., 2024a; Ai et al., 2024b; Alamdar et al., 2012; Alvandi and Ardestani, 2023; Chen et al., 2017; Cooper and Cowan, 2006; Ekinci et al., 2013; Evjen, 1936; Fedi and Florio, 2001; Ferreira et al., 2013; Li et al., 2013; Miller and Singh, 1994; Nasuti and Nasuti, 2018; Sun et al., 2016; Wijns et al., 2005).

This study aimed to detect potential structure distribution in the southeastern Aegean region based on gravity data, providing a detailed seismotectonic map. To this end, data processing and detecting the edges of the potential structures were completed in this study. The gravity dataset was compiled from the TOPEX v29.1 database (Sandwell et al., 2013; Sandwell et al., 2014; Sandwell and Smith, 2009; Smith and Sandwell, 1997). Fast Sigmoid (FSED) and the Tilt angle of the Total Horizontal Gradient (TAHG) methods have been selected because of their accuracy in detecting lateral boundaries of the causative structures. Moreover, we evaluated whether the potential structures are faults. For this reason, we compiled a homogenized fault map using existing fault catalogs (which are the Eurasia database (AFEAD), European Fault – Source Model 2020 (EFSM20), and (NOAFAULTs)), which were then compared to the edge detection maps we generated (Basili et al., 2023; Basili et al., 2022; Ganas et al., 2013; Zelenin et al., 2021). Through correlation with seismological data, an interpretation was made. This approach has allowed for a detailed visualization of the seismotectonic features of the region. In our study, the FSED and TAHG methods produced distinct results in identifying anomalies related to the existing faults. The FSED method showed a stronger alignment with the faults, while the TAHG method generated fault-independent anomalies in certain areas. This suggests that the two methods are sensitive to different deformation processes or the variable characteristics of subsurface structures.

2. Seismicity of the Study Area

The study area is between 35.5°N and 38.5°N in latitude and 26°E and 29°E in longitude. The earthquake catalog data for the study area were compiled from the Disaster and Emergency Management Presidency (AFAD), Boğaziçi University Kandilli Observatory and Earthquake Research Institute – Regional Earthquake-Tsunami Monitoring Center (B.U.KOERI-RETMC), the Geodynamics Institute of the National Observatory of Athens (GI-NOA, http://www.gein.noa.gr/services/cat.htm) and United States Geological Survey (USGS) earthquake catalogs (https://earthquake.usgs.gov/earthquakes/search/). The compiled catalog contains 92067 earthquakes with magnitudes of $0.0 \leq Mw \leq 7.2$ from 1900 to August 31, 2023. Twenty-four earthquakes are with magnitudes $Mw \geq 6.0$. The last earthquakes, with a magnitude of $Mw = 6.6$ Bodrum-Kos earthquake on July 20, 2017 (Cordrie et al., 2021; Dimova and Raykova, 2018; Dogan et al., 2018; Dogan et al., 2019; Ganas et al., 2019; Heidarzadeh et al., 2017; Karakostas et al., 2022; Karasözen et al., 2018; Konca et al., 2019; Över et al., 2021; Öztürk and Şahin, 2019; Papadopoulos et al., 2019; Papathanassiou et al., 2019; Sboras et al., 2020; Tiryakioğlu et al., 2018), and the $Mw = 6.9$ Samos earthquake on October 30, 2020 (Akinci et al., 2021; Aktas et al., 2022; Chousianitis and Konca, 2021; Hu et al., 2022; Karakostas et al., 2021; Kiratzi et al., 2021; Sboras et al., 2021; Sun et al., 2024; Taymaz et al., 2022). According to the depth analysis visualized with the ZMAP program (Wiemer, 2001), the depths of the earthquakes occurring in the study region, including these, are between 0 and 192 km. The zone between 0-35 km is seismically very active: 97% of the earthquakes occurred in the first 35 km depth. $Mw \geq 6.0$ earthquakes occur at 0-100 km depths, and $Mw \geq 5.0$ earthquakes occur at depths up to 192 km (Fig. 2a). Most seismic activity in the SE Aegean occurs around Samos

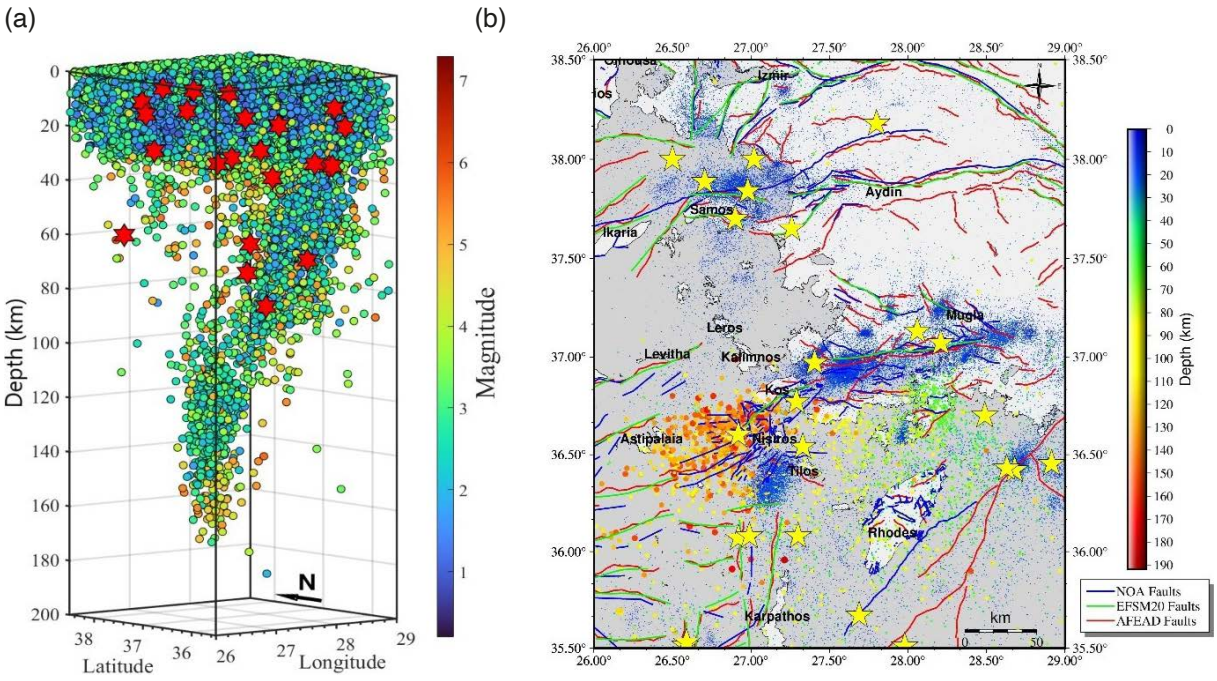

Figure 2. (a) 3D spatial distribution of the earthquakes by magnitudes in the depth section (red stars represent Mw ≥ 6.0 earthquakes) (This map was produced by ZMAP), (b) The epicenter distribution of the earthquakes (yellow stars represent Mw ≥ 6.0 earthquakes) (This map was produced by GMT v6.5).

Island and in the Gulf of Gökova. The majority of earthquakes in these regions occur at depths between 0-40 km. However, the earthquake depths in Gökova Bay and its southern area reach 80 km. According to the map plotted by the GMT 6 program (Wessel et al., 2019), the epicenter distributions of earthquakes deeper than 120 km to 192 km are concentrated between coordinates 36-36.8°N and 26-27°E (Fig. 2b). Deep earthquakes occur in the region due to the subduction of the African Plate under the Aegean.

According to the historical earthquake catalogs (the European Archive of Historical Earthquake Data (AHEAD), Share European Earthquake Catalog (SHEEC) and Disaster and Emergency Management Presidency (AFAD) (https://deprem.afad.gov.tr/event-historical)), 195 earthquakes occurred in the region throughout the historical period (Albini et al., 2013; Stucchi et al., 2013). The maximum observed macroseismic intensity (historical magnitude) of the earthquakes between 1040 and 1899 varied between IV and X, and many of the largest historical earthquakes in the Aegean Sea were destructive earthquakes in tsunami catalogs.

3. Data and Methods

There are several established methods for edge detection, including the Analytic Signal (ASA), First Order Vertical Derivative (VDR), Total Horizontal Derivative (THDR), Tilt Angle (TA), and Theta Map techniques. In this study, we have chosen the Fast Sigmoid (FSED) and Tilt Angle of Horizontal Gradient (TAHG) methods due to their superior ability to identify potential source edges at their maximum values, as well as their effectiveness in balancing anomalies originating from both deep and shallow geological sources. When compared to traditional edge detection methods, both FSED and TAHG have shown improved performance. The boundaries of potential tectonic structures have been settled over and around the maximum values of both methods (Altinoğlu, 2023; Eldosouky et al., 2022; Ferreira et al., 2013; Oksum et al., 2021).

Oksum et al. (2021) proposed the Fast Sigmoid method to estimate the edges of potential structures from the total horizontal gradient of potential field anomalies. This method uses a modified fast sigmoid function of R and is defined as

$$FSED = \frac{R-1}{1+|R|} \tag{1}$$

where R is the ratio of the first-order vertical and horizontal derivatives of the total horizontal gradient of the potential field and is calculated as follows:

$$R = \frac{\frac{\partial THDR}{\partial z}}{\sqrt{\left(\frac{\partial THDR}{\partial x}\right)^2 + \left(\frac{\partial THDR}{\partial y}\right)^2}} \tag{2}$$

In addition to the FSED method, we used the Tilt angle of the horizontal gradient (TAHG) method. Ferreira et al. (2013) developed this method, which involves calculating the arctangent of the vertical derivative of the total horizontal gradient (THDR) divided by the THDR's modulus. The properties of arctangent result in the TAHG transform ranging between $-\pi/2$ and $\pi/2$. The TAHG method is described as follows:

$$TAHG = tan^{-1}\left(\frac{\frac{\partial THDR}{\partial z}}{\sqrt{\left(\frac{\partial THDR}{\partial x}\right)^2 + \left(\frac{\partial THDR}{\partial y}\right)^2}}\right) \tag{3}$$

4. Application to Synthetic Data

In this section, we applied the TAHG and FSED methods to a 3D synthetic model to evaluate their effectiveness. We generated a gravimetric model composed of five prisms, as shown in Fig. 3. Figures 3a and 3b present three-dimensional and planar views of the synthetic model, respectively. The prismatic model blocks are positioned at different locations and contain negative and positive density contrasts. The geometric parameters and density contrast values of the synthetic model are shown in Table 1. The gravity anomalies due to the five prisms were calculated on a grid of 16 km × 14 km points, with a spatial resolution of 1000 m (Fig. 4a). To assess the performance of the filters in field gravity data, we added random noise of 2% to the synthetic gravity anomalies in Fig. 4a. Figure 4b presents noise-corrupted synthetic gravity anomalies. An upward continuation filter of 200 m was applied to the noise-corrupted synthetic gravity anomalies to reduce the residual components and better visualize the

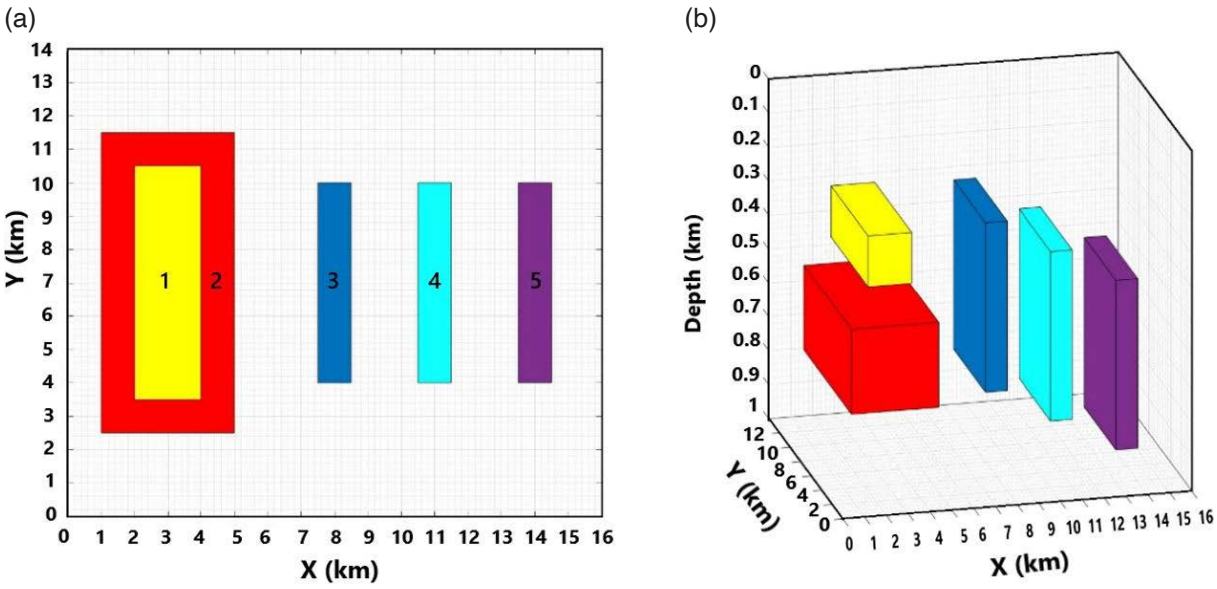

Figure 3. Model: (a) Planar view, (b) Three-dimensional view.

Prismatic bodies	1	2	3	4	5
x coordinates (m)	3000	3000	8000	11000	14000
y coordinates (m)	7000	7000	7000	7000	7000
Depth of top (m)	250	500	250	350	450
Prism Thickness (m)	150	250	500	500	500
Prism Length (m)	7000	9000	6000	6000	6000
Prism Width (m)	2000	4000	1000	1000	1000
Density contrast (kg/m^3)	3500	-3000	2000	-2000	2000

Table 1. Geometric parameters and density contrast values of the synthetic model.

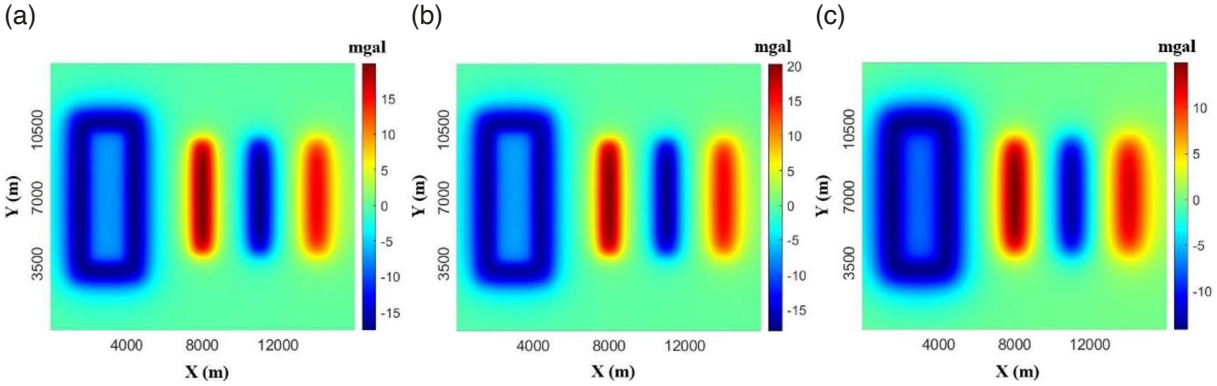

Figure 4. (a) Gravity anomaly of the model in Fig. 3, (b) Gravity anomaly corrupted by uniformly distributed random noise, (c) Noisy gravity anomaly upward continued to 200 m.

boundaries of prismatic sources. Figure 4c shows the noisy gravity anomaly upward continued to 200 m. Figure 5a-b depicts the results obtained from the application of the TAHG and FSED methods, respectively, to the synthetic gravity anomaly (Figs. 5a, 5c) and the noisy synthetic anomaly after applying an upward continuation filter to 200 m (Figs. 5b, 5d). According to the results of both methods, the maxima values depict the edges of the sources. Although the TAHG is able to balance the anomaly amplitudes of source prisms with different depth values, it has resolution problems around the sources. The edges of all sources by the TAHG are enhanced in a noise-free environment, whereas the edges of sources 1 and 2 are not well defined in the noisy environment. Edges of sources 3, 4, and 5 are defined as blurred. On the other hand, the FSED method sharpens and highlights the source edges with better resolution for all prisms.

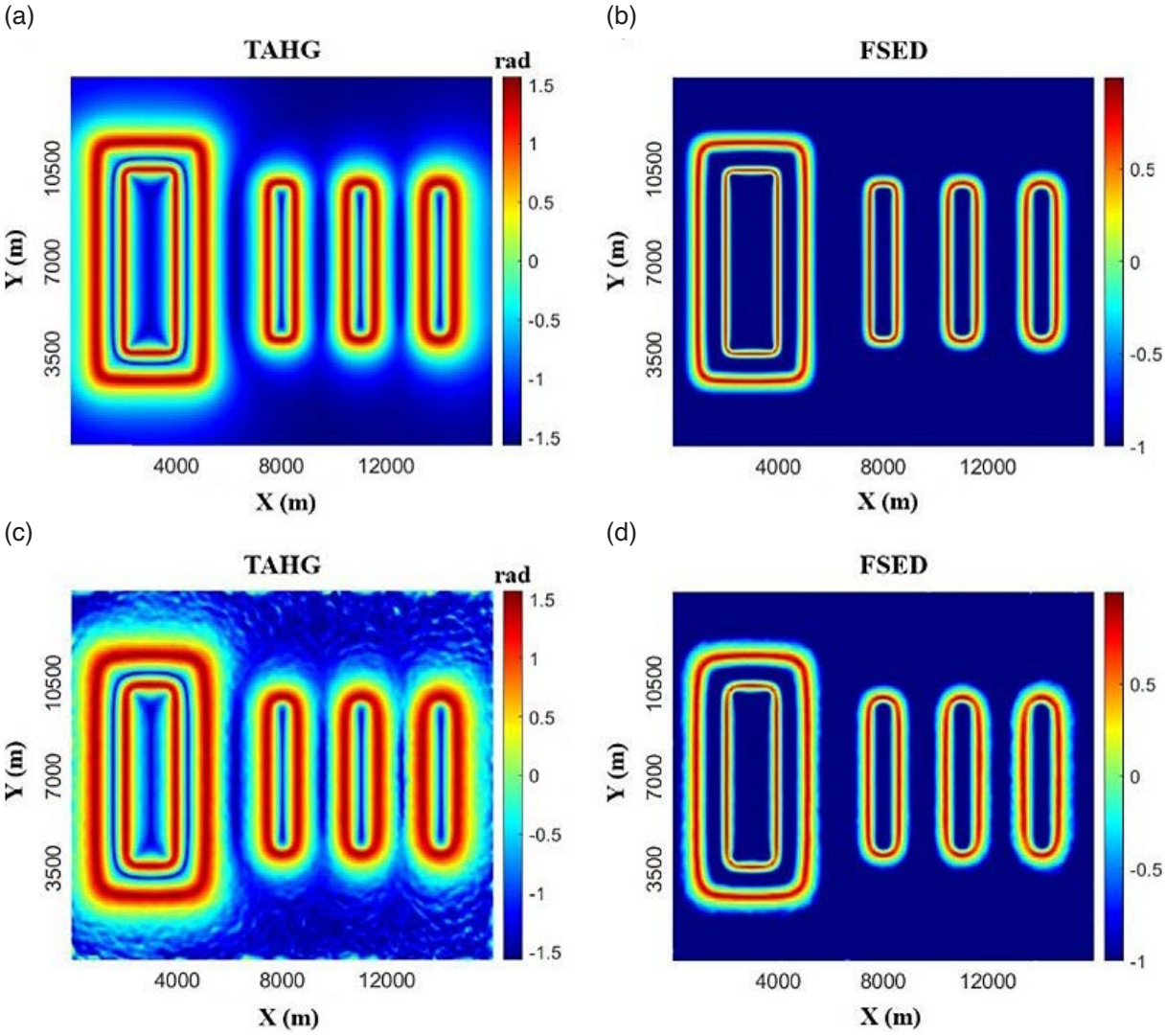

Figure 5. For the synthetic model in Fig. 3: (a) TAHG for noise-free data, (b) FSED for the noise-free anomaly, (c) TAHG for noisy gravity anomaly upward continued to 200 m, (d) FSED for noisy gravity anomaly upward continued to 200 m.

5. Application to Gravity Data

Currently, there are many datasets available as open sources, such as WGM2012 (Bonvalot et al., 2012) and EGM2008 (Pavlis et al., 2012), for the analysis of potential structures. Bouguer gravity maps of the desired coordinates can be obtained by means of these datasets. The dataset used in this study is gravity data from global 1-minute grids from the TOPEX v29.1 database. TOPEX primarily provides gravity data related to the ocean surface and seafloor. These data are highly valuable for the study of seafloor structures, ocean currents, sea level changes, and other oceanic dynamics. Satellite data, such as those from TOPEX, offer precise measurements of sea surface gravity and provide more detailed information through modeling of these data. In particular, in oceanic regions, the resolution of gravity anomalies on the seafloor can significantly aid in the clearer identification of underwater features. Since our study area includes a significant portion of marine regions, we preferred TOPEX gravity data, which is altimetry-based and provides high-resolution gravity anomalies in oceanic and seafloor regions. In contrast, WGM 2012 is derived from multiple sources (satellite, terrestrial, and shipborne data) but is not directly altimetry-based, while EGM 2008 is a global geoid model and may not be as suitable for detailed local analyses. Given these considerations, TOPEX data was the most appropriate choice for our study area. Research utilizing the TOPEX database can be given, such as Gönenç (2021) examining the availability of TOPEX V28.1 gravity data across continents excluding seas. Moreover, Putri et al. (2019) present new research in the field of environmental sciences. The gravity data provided are already free-air data, so we need to apply terrain correction to generate the Bouguer anomaly. The terrain correction

relies on topographic data, which are also supplied by the same database. Terrain correction and regional residual separation were performed using the Geosoft Oasis Montaj (Geosoft Inc., 2015). The density value utilized for Bouguer correction was determined to be 2.67 g/cm^3. As deep structures were the focus of the study, edge detection methods were applied to the regional map. The upward continuation method is employed in Bouguer anomaly mapping to reduce noise and achieve a smoother representation before engaging in edge detection processes, aiming to yield more effective results. Various elevation values were tested for upward continuation processes to ensure minimal data loss, with the optimal value observed to be 3500 m. An upward continuation of 3500 m was applied to the regional map, and the gravity map was prepared for edge detection (Fig. 6).

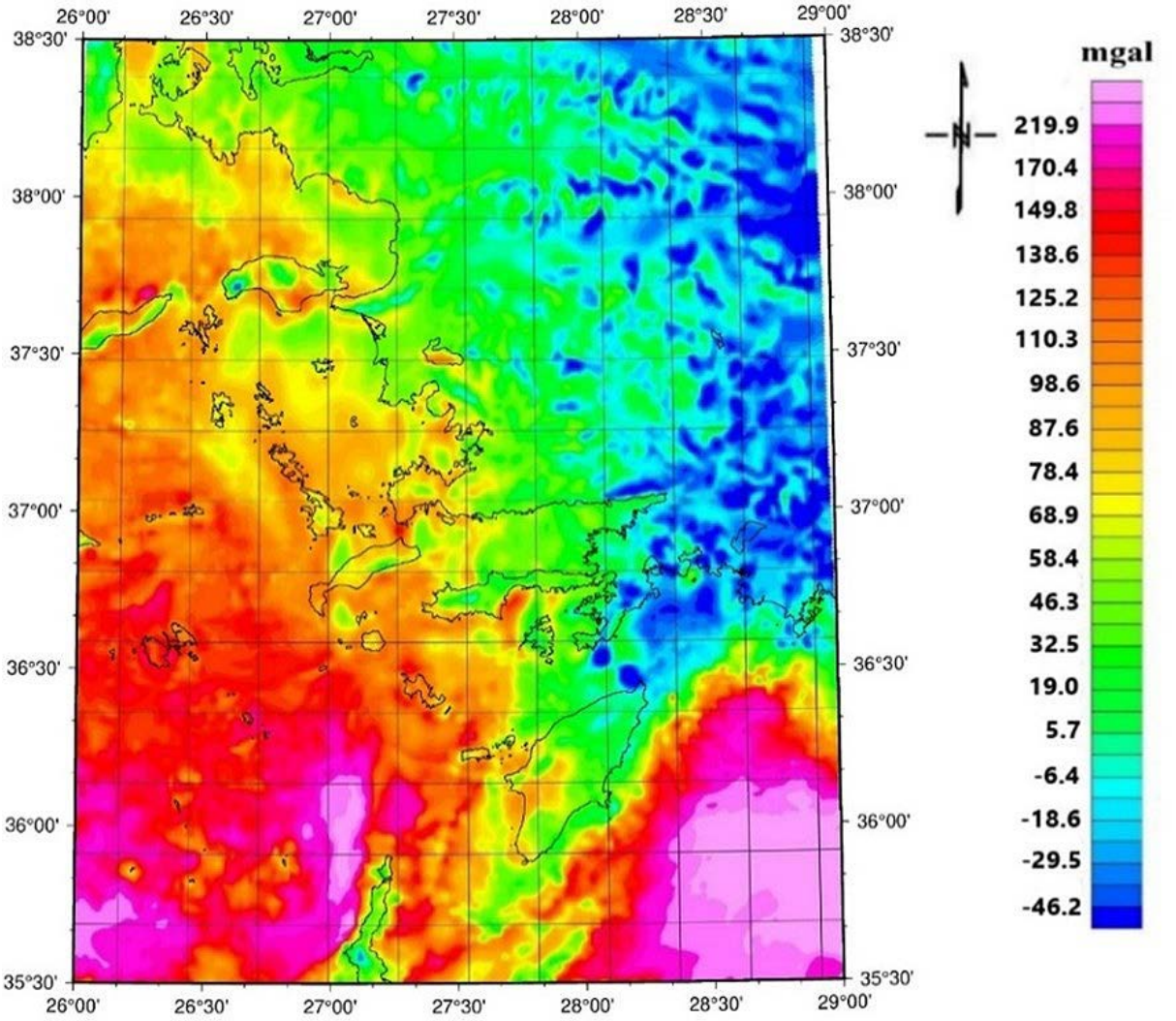

Figure 6. Regional gravity anomaly map of the survey area.

6. Results and Discussion

Figures 7a and 7b present the anomaly maps generated using the FSED and TAHG methods to identify potential structure boundaries. These boundaries, numbered 1 to 69, are shown with dashed lines in Figs. 8a and 8b. In the FSED map, anomalies with maximum values (approximately 0.8365) are considered potential structure boundaries (Fig. 8a), some of which may indicate potential fault locations. In cases where seismic activity is also high at the structure boundaries where high-value anomalies are located, it is thought that these structures may be potential faults (Fig. 10). If the anomaly values were high, regardless of whether the seismic activity was low or high, the presence of seismic activity ensured that the structure boundary was accepted as a potential fault (fault

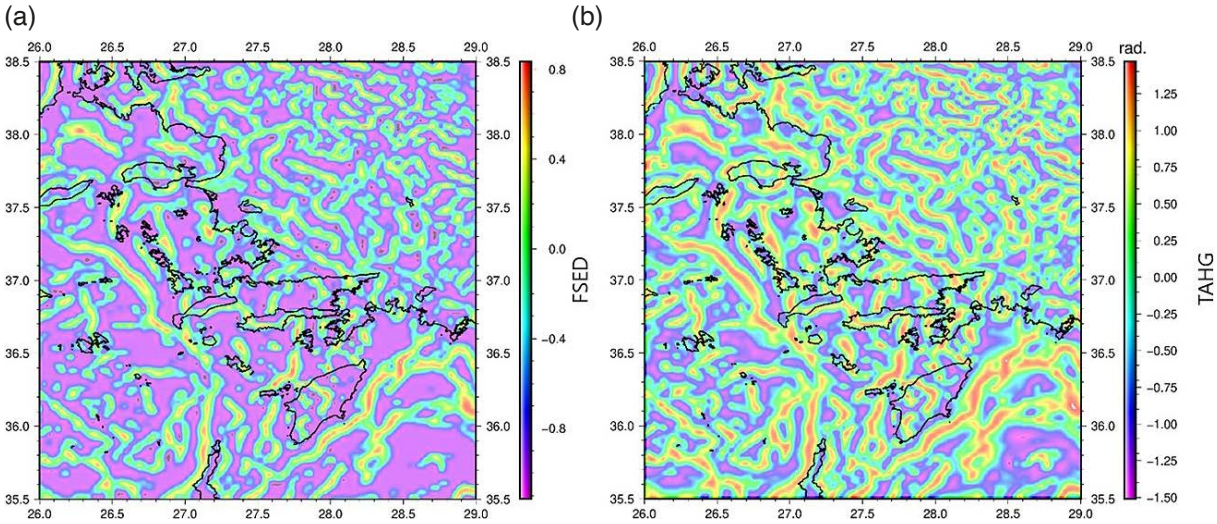

Figure 7. (a) FSED map, (b) TAHG map (solid lines show coastlines).

numbers 1, 6, 15, 27, 30, 39, 43, 53 and 69). Moreover, anomalies with high values but no seismic activity were observed. Since these faults are located in the continuations of existing faults, they were accepted as potential faults (fault numbers 40 and 42). Structure boundaries with high anomaly values and seismic activity were identified as potential faults related to existing faults (e.g., faults numbered 7, 10, 38, 40, 42, 43, 44 and 62).

Since anomaly data alone cannot precisely define fault orientations, a few existing focal mechanism solutions were used to confirm potential fault directions. The focal mechanisms are compiled from AFAD, B.U.KOERI-RETMC, the GEOFON data center of the GFZ German Research Centre for Geosciences and the Global Centroid-Moment-Tensor (GCMT) project catalogs (Dziewonski et al., 1981; Ekström et al., 2012). Based on the existing focal mechanism solution available for the location of anomaly number 44, the potential fault's orientation at this anomaly can be northeast-southwest. This fault can be the continuation of the northeast-southwest trending fault listed in the NOAFAULTs database. The earthquake's focal mechanism on potential fault number 20 indicates that the fault orientation is northwest-southeast. The directions of the anomalies belonging to both potential fault boundaries, numbered 44 and 20, are compared to the strike of the focal mechanisms on these anomaly locations; it is seen that they are compatible. Likewise, the directions of the anomalies thought to be possible fault locations

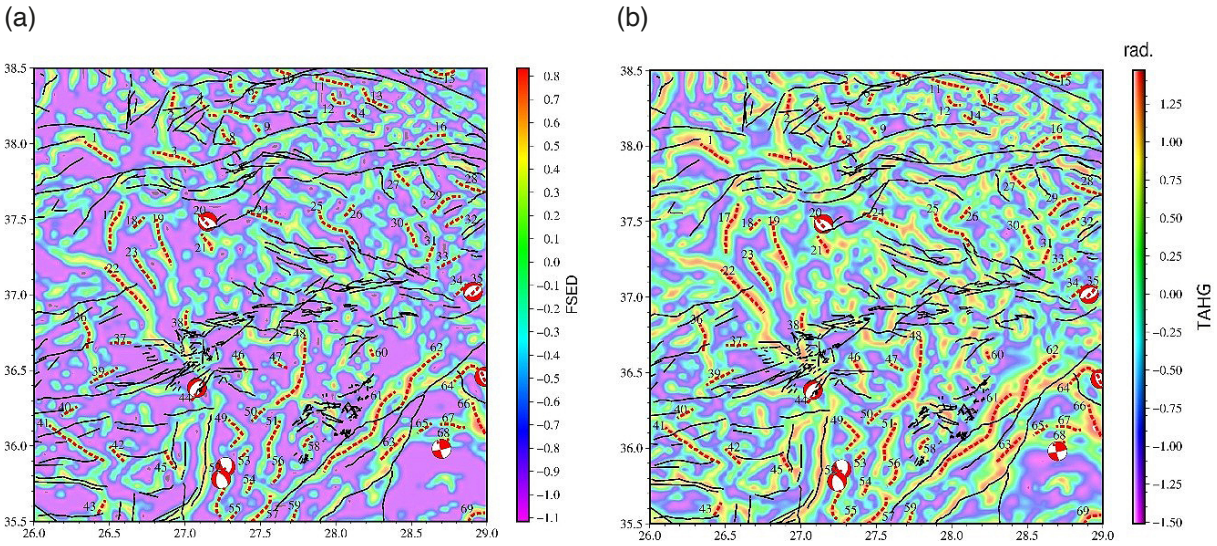

Figure 8. (a) Potential structure boundaries on the FSED map, (b) Potential structure boundaries on the TAHG map (red dashed lines, solid black lines and red beach balls represent detected structure boundaries, existing faults and focal mechanisms, respectively.)

numbered 35, 52, 64 and 68 are compatible with the strike of earthquakes in these locations by the few focal mechanisms. The boundaries of the structures identified as potential faults are generally located in areas with earthquakes at focal depths of 0-30 km (Fig. 9). These potential faults are also observed in regions with earthquakes at depths of 100-120 km (37, 38, and 39). Some of these faults are situated close to the epicenters of earthquakes with magnitudes of M ≥ 6.0 (1, 3, 49, and 64). Structure boundaries showing high anomaly values and quite large boundaries were detected where earthquakes occurred at depths between 40 and 100 km (48, 51, 61 and 62).

The anomalies with maximum values (approximately 1.4793) were considered potential fault locations in the TAHG method (Fig. 8b). A total of 69 potential structure boundaries were detected by the FSED method and were also identified by the TAHG method. Both methods successfully identify potential structure boundaries, yet the anomalies obtained with the FSED method allow for more detailed interpretations with higher resolution.

The boundaries determined using the FSED method were compared with those defined by the TAHG method. Anomalies observed using the TAHG method exhibited higher values than those from the FSED method and were more distinct and continuous. The boundaries appearing as two separate anomalies in the FSED method were seen

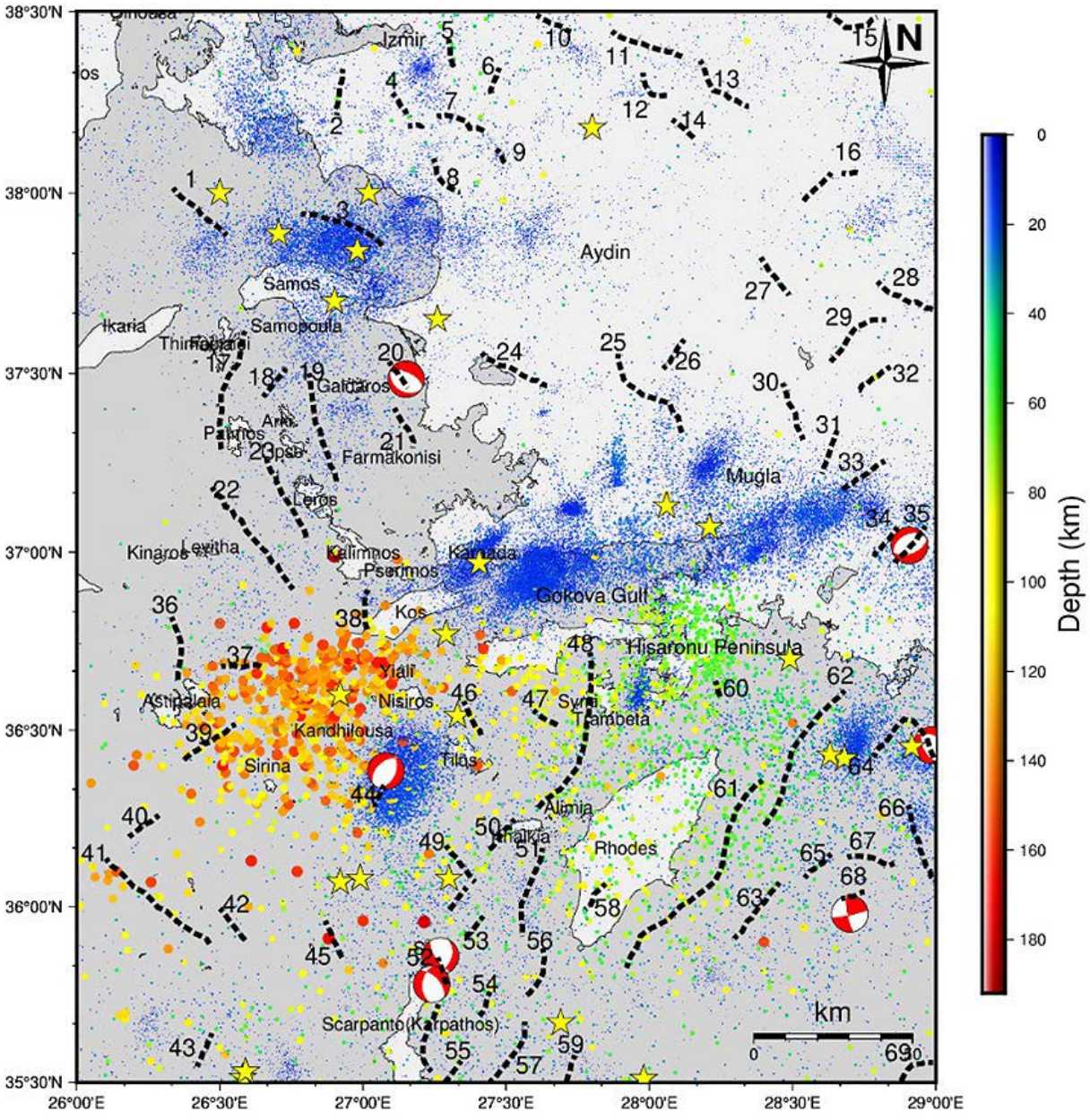

Figure 9. Interpretation map (potential structure boundaries, focal mechanisms, earthquakes larger than M ≥ 6.0 and circles are shown by dashed lines, red beach balls, yellow stars and circles colored by their depth, respectively).

as single anomalies with larger sizes in the TAHG method. While anomaly 41 is separated in the map obtained by the FSED method, it shows continuity in the TAHG map. The boundaries of this anomaly cut existing faults. The potential structural boundaries causing high anomalies in the region where deep earthquakes occur should be interpreted together with other geophysical methods.

The map in Fig. 10 comprehensively visualizes the identified potential structure boundaries, including potential fault locations (dashed lines) and existing faults (solid lines). Integrating seismicity and focal mechanisms with gravity anomaly data offers a robust framework for correlating these structural boundaries with seismic activity, enabling a more detailed and accurate mapping of potential fault structures crucial for understanding the region's tectonic behavior.

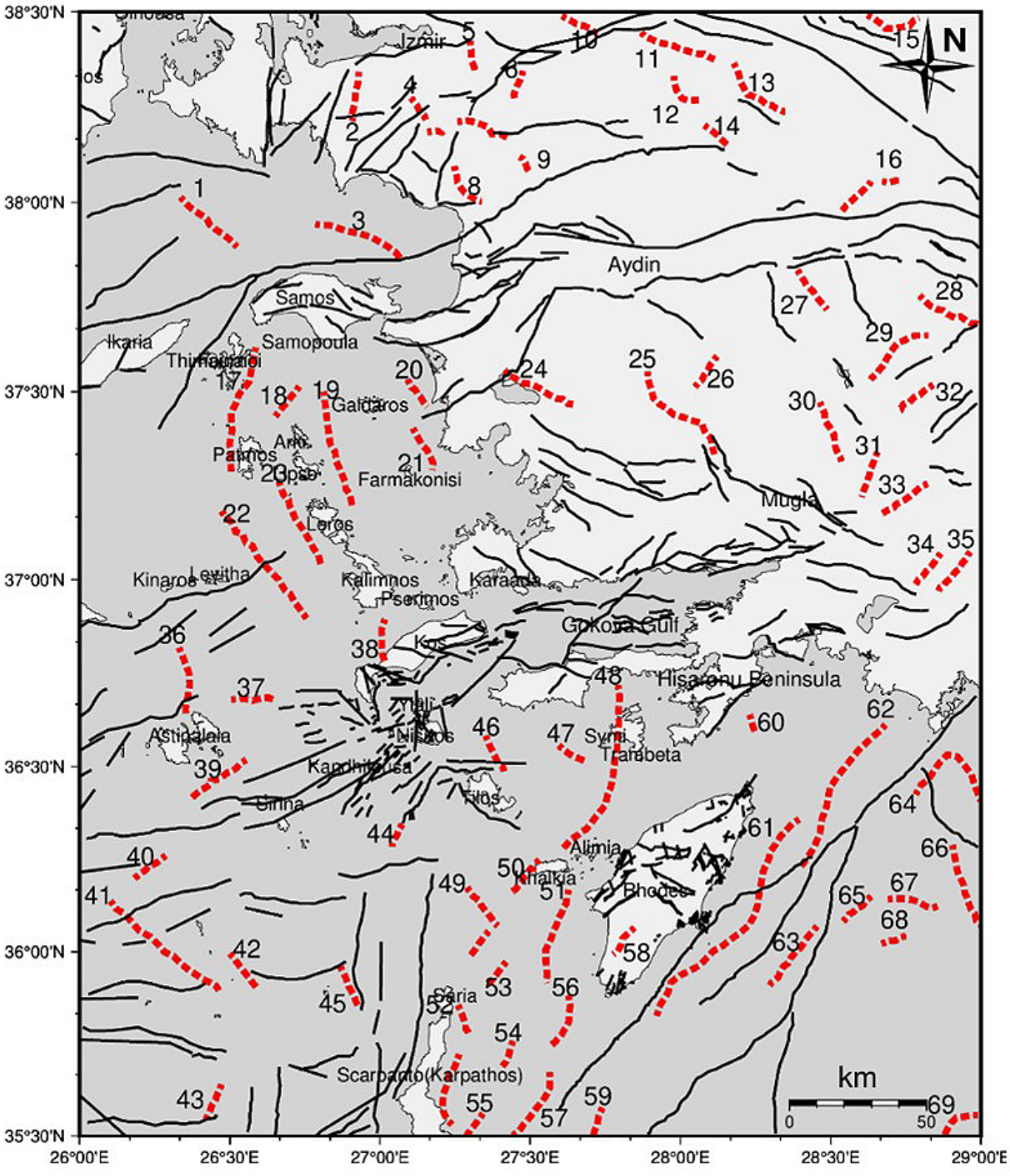

Figure 10. Final interpretation map (potential structure boundaries and existing fault lines are shown by dashed lines and solid lines, respectively.)

7. Conclusions

This research comprehensively investigates the fault structures in the southeastern Aegean region, a region of significant seismotectonic complexity. This study identifies numerous potential structures by utilizing gravity data from the TOPEX v29.1 database and applying the Fast Sigmoid Edge Detection (FSED) and Tilt Angle of the Total Horizontal Gradient (TAHG) methods. The detected features show strong alignment with established databases such as AFEAD, EFSM20, and NOAFAULTs, reinforcing the validity of these methods.

The higher overlap of the FSED method with the faults indicates that this approach is more likely to align with local deformation structures. On the other hand, the TAHG method produced fault-independent anomalies in specific regions, which may provide additional insights into stress distribution beyond fault zones and the detection of regional deformations. To assess the success of these methods, statistical correlation analyses, comparisons with different geophysical parameters, and validations with geological field observations can be performed. Our study suggests that such methods should not be used in isolation, but rather as complementary analyses. In line with this, we have correlated the results obtained from the edge-detection with seismological data to provide a more comprehensive interpretation. The integration of the seismicity and focal mechanisms of earthquakes provided a robust framework for correlating gravity anomalies with seismic activity. This comprehensive approach ensures a more detailed and accurate mapping of fault structures is crucial for understanding the tectonic behavior of the region.

It is not realistic to expect the existing faults in the databases to perfectly coincide with the detected anomalies. Gravity anomalies are sensitive to density contrasts. If there is no significant density contrast along a fault, the fault may not be clearly visible in the gravity data. Particularly for strike-slip faults, which do not involve significant vertical displacement, gravity anomalies may be weak or absent. Some faults may have been active in the past but are no longer seismically active, leading to weak gravity signals. Conversely, some anomalies may appear in regions different from mapped faults, potentially indicating previously unidentified subsurface structures.

One of the key contributions of this study is the detailed mapping of potential structure edges using advanced edge detection techniques. These methods, particularly when combined, offer enhanced resolution and accuracy, highlighting their effectiveness in geophysical research.

Furthermore, this study emphasizes the dynamic nature of the tectonics of the southeastern Aegean region, which is influenced by complex interactions among the African, Eurasian, and Anatolian plates. The findings suggest that the addition of newly identified faults to existing databases can significantly improve the precision of seismic hazard models and risk assessments in the region.

In conclusion, the integration of advanced geophysical techniques, comprehensive seismic activity, and focal mechanism data for earthquakes has significantly contributed to understanding fault dynamics and seismic hazards in the southern Aegean region. This approach not only enhances the geological and seismological knowledge of the area but also provides a robust foundation for future research and practical applications in seismic hazard management.

Acknowledgments. The authors thank Dr. Ahmad Alvandi and the reviewers for their valuable and constructive comments on this work.

References

Ai, H., Y. L. Ekinci, A. Alvandi, H. Deniz Toktay et al. (2024a). Detecting edges of geologic sources from gravity or magnetic anomalies through a novel algorithm based on hyperbolic tangent function, Turk. J. Earth. Sci., 33, 6, doi:10.55730/1300-0985.1936.

Ai, H., H. Deniz Toktay, A. Alvandi, R. Pašteka et al. (2024b). Advancing potential field data analysis: the Modified Horizontal Gradient Amplitude method (MHGA), Contrib. Geophys. Geodes., 54, 2, 119-143, doi:10.31577/congeo.2024.54.2.1.

Akinci, A., D. Cheloni and A. A. Dindar (2021). The 30 October 2020, M7.0 Samos Island (Eastern Aegean Sea) Earthquake: effects of source rupture, path and local-site conditions on the observed and simulated ground motions, B. Earthq. Eng., 19, 4745-4771, doi:10.1007/s10518-021-01146-5.

Aktas, Y. D., I. Ioannou, F. S. Malcioglu, A. P. Vatteri et al. (2022). Traditional Structures in Turkey and Greece in 30 October 2020 Aegean Sea Earthquake: Field Observations and Empirical Fragility Assessment, Front. Built Environ., 8, 840159, doi:10.3389/fbuil.2022.840159.

Alamdar, K., A. Kamkare Rouhani and H. Ansari (2012). A new edge detection method based on the analytic signal of tilt angle (ASTA) for magnetic anomalies, In: Istanbul 2012-International Geophysical Conference and Oil & Gas Exhibition.

Albini, P., M. Locati, A. Rovida and M. Stucchi (2013). European Archive of Historical EArthquake Data (AHEAD), Istituto Nazionale di Geofisica e Vulcanologia (INGV).

Altinoğlu, F. F. (2023). Mapping of the structural lineaments and sedimentary basement relief using gravity data to guide mineral exploration in the Denizli Basin, Minerals, 13, 10, 1276, doi:10.3390/min13101276.

Altınok, Y. and Ş. Ersoy (2000). Tsunamis observed on and near the Turkish coast, Nat. Hazards: State-of-the-Art at the End of the Second Millennium, 185-205, doi:10.1023/A:1008155117243.

Alvandi, A. and V. Ardestani (2023). Edge detection of potential field anomalies using the Gompertz function as a high-resolution edge enhancement filter, B. Geophys. Oceanogr. (BGO), 64, 3, doi:10.4430/bgo00420.

Ambraseys, N. and C. Synolakis (2010). Tsunami catalogs for the Eastern Mediterranean, revisited, J. Earthquake Eng., 14, 3, 309-330, doi:10.1080/13632460903277593.

Andinisari, R., K. Konstantinou and P. Ranjan (2020). Seismotectonics of SE Aegean inferred from precise relative locations of shallow crustal earthquakes, J. Seismol., 24, 1, 1-22, doi:10.1007/s10950-019-09881-8.

Baker, C., D. L. Hatzfeld, H. Lyon-Caen, E. Papadimitriou et al. (1997). Earthquake mechanisms of the Adriatic Sea and Western Greece: implications for the oceanic subduction-continental collision transition, Geophys. J. Int., 131, 3, 559-594, doi:10.1111/j.1365-246X.1997.tb06600.x.

Basili, R., L. Danciu, C. Beauval, K. Sesetyan et al. (2023). The European Fault-Source Model 2020 (EFSM20): geologic input data for the European Seismic Hazard Model 2020, Nat. Hazards Earth Syst. Sci. Discuss., 2023, 1-44, doi:10.5194/nhess-24-3945-2024.

Basili, R., L. Danciu, C. Beauval, K. Şeşetyan et al. (2022). European fault-source model 2020 (EFSM20): Online data on fault geometry and activity parameters [data set], Istituto Nazionale di Geofisica e Vulcanologia (INGV), doi:10.13127/efsm20.

Brun, J.-P., F. Gueydan, D. Sokoutis, M. Philippon et al. (2017). Effects of slab rollback acceleration on Aegean extension, Bul. Geol. Soc. Greece, 50, 1, 5-23, doi:10.12681/bgsg.11697.

Cambaz, M. D. and A. K. Mutlu (2016). Regional moment tensor inversion for earthquakes in Turkey and its surroundings: 2008-2015, Seismol. Res. Lett., 87, 5, 1082-1090, doi:10.1785/0220150276.

Chen, A.-G., Z. Tao-Fa, L. Dong-Jia and Z. Shu (2017). Application of an enhanced theta-based filter for potential field edge detection: a case study of the Luzong Ore District, Chin. J. Geophys., 60, 2, 203-218, doi:10.1002/cjg2.30039.

Chousianitis, K. and A. O. Konca (2021). Rupture process of the 2020 Mw 7.0 Samos earthquake and its effect on surrounding active faults, Geophys. Res. Lett., 48, 14, e2021GL094162, doi:10.1029/2021GL094162.

Cooper, G., and D. Cowan (2006). Enhancing potential field data using filters based on the local phase, Comput. Geosci., 32, 10, 1585-1591, doi:10.1016/j.cageo.2006.02.016.

Cordrie, L., A. Gailler, P. Heinrich, P. Briole et al. (2021). The July 20, 2017 Mw = 6.6 Bodrum-Kos earthquake, Southeast Aegean Sea: Contribution of the tsunami modeling to the assessment of the fault parameters, Pure Appl. Geophys., 178, 12, 4865-4889, doi:10.1007/s00024-021-02766-3.

Delibasis, N. (1968). Focal mechanism of earthquakes of intermediate focal depth in the arc of Greece and the distribution of their macroseismic intensities (Unpublished doctoral dissertation). Univ. Athens.

Dewey, J. and A. Şengör (1979). Aegean and surrounding regions: complex multiplate and continuum tectonics in a convergent zone, Geol. Soc. Am. Bull., 90, 1, 84-92, doi:10.1130/0016-7606(1979)90<84:AASRCM>2.0.CO;2.

Di Maro, R. and A. Maramai (1992). Tsunamis in the Mediterranean and Pacific areas: an analysis, Sci. Tsunami Hazards, 10, 1, 35-49.

Dimova, L. and R. Raykova (2018). Numerical simulations of the earthquake-induced tsunami of July 20, 2017 (Mw = 6.6) in Bodrum-Kos, Aegean Sea, Rev. Bulg. Geol. Soc., 79, 1, 5-12.

Dogan, A. H., N. Tunalioglu, B. Erdogan and T. Ocalan (2018). Evaluation of the GPS Precise Point Positioning technique during the 21 July 2017 Kos-Bodrum (East Aegean Sea) Mw 6.6 earthquake, Arab. J. Geosci., 11, 1-10, doi:10.1007/s12517-018-4140-z.

Dogan, G. G., A. Annunziato, G. A. Papadopoulos, H. G. Guler et al. (2019). The 20th July 2017 Bodrum-Kos Tsunami Field Survey, Pure Appl. Geophys., 176, 2925-2949, doi:10.1007/s00024-019-02151-1.

Dogan, G. G., A. C. Yalciner, Y. Yuksel, E. Ulutaş et al. (2021). The 30 October 2020 Aegean Sea tsunami: post-event field survey along Turkish coast, Pure Appl. Geophys., 178, 785-812, doi:10.1007/s00024-021-02693-3.

Doglioni, C., S. Agostini, M. Crespi, F. Innocenti et al. (2002). On the extension in western Anatolia and the Aegean Sea, J. Virtual Explor., 8, 169-183, doi:10.3809/jvirtex.2002.00049.

Dominey-Howes, D. (2002). Documentary and Geological Records of Tsunamis in the Aegean Sea Region of Greece and their Potential Value to Risk Assessment and Disaster Management, Nat. Hazards, 25, 195-224, doi:10.1023/A:1014808804611.

Dominey-Howes, D., G. Papadopoulos and A. Dawson (2000). Geological and historical investigation of the 1650 Mt. Columbo (Thera Island) eruption and tsunami, Aegean Sea, Greece, Nat. Hazards, 21, 83-96, doi:10.1023/A:1008178100633.

Dziewonski, A. M., T. A. Chou and J. H. Woodhouse (1981). Determination of earthquake source parameters from waveform data for studies of global and regional seismicity, JGR: Solid Earth, 86, B4, 2825-2852, doi:10.1029/JB086iB04p02825.

Ekinci, Y. L., C. Ertekin and E. Yiğitbaş (2013). On the effectiveness of directional derivative based filters on gravity anomalies for source edge approximation: synthetic simulations and a case study from the Aegean graben system (western Anatolia, Turkey), J. Geophys. Eng., 10, 3, 035005, doi:10.1088/1742-2132/10/3/035005.

Ekström, G., M. Nettles and A. Dziewoński (2012). The global CMT project 2004-2010: Centroid-moment tensors for 13,017 earthquakes, Phys. Earth Planet. Inter., 200, 1-9, doi:10.1016/j.pepi.2012.04.002.

Eldosouky, A. M., L. T. Pham, V.-H. Duong, F. E. Kemgang Ghomsi et al. (2022). Structural interpretation of potential field data using the enhancement techniques: a case study, Geocart. Internat., 37, 27, 16900-16925, doi:10.1080/10106049.2022.2120548.

Emre, O., S. Ozalp and T. Duman (2011). 1:250,000 scale active fault map series of Turkey, Izmir (NJ 35-7) Quadrangle. Serial number: 6.

Evjen, H. M. (1936). The place of the vertical gradient in gravitational interpretations, Geophysics, 1, 1, 127-136, doi:10.1190/1.1437067.

Eyidoğan, H. (2022). Ege Denizi Güney İncirli Havzası Deprem Fırtınasının Sismolojik ve Sismotektonik Özellikleri, Turk. J. Earth. Sci., 4, 1, doi:10.46464/tdad.1024334.

Fedi, M. and G. Florio (2001). Detection of potential fields source boundaries by enhanced horizontal derivative method, Geophys. Prospect., 49, 1, 40-58, doi:10.1046/j.1365-2478.2001.00235.x.

Ferreira, F. J., J. de Souza, J., A. de B. e S. Bongiolo and L. G. de Castro (2013). Enhancement of the total horizontal gradient of magnetic anomalies using the tilt angle, Geophysics, 78, 3, J33-J41, doi:10.1190/geo2011-0441.1.

Friederich, W., A. Brüstle, L. Küperkoch and T. Meier (2013). Focal mechanisms in the Southern Aegean from temporary seismic networks-implications for the regional stress field and ongoing deformation processes, Solid Earth Discuss., 5, 2, doi:10.5194/sed-5-1721-2013.

Galanopoulos, A. G. (1960). Tsunamis observed on the coasts of Greece from antiquity to present time, Ann. Geophys., 13, 3-4, 369-386, doi:10.4401/ag-5477.

Ganas, A., P. Elias, V. Kapetanidis, S. Valkaniotis et al. (2019). The July 20, 2017 M6. 6 Kos earthquake: seismic and geodetic evidence for an active north-dipping normal fault at the western end of the Gulf of Gökova (SE Aegean Sea), Pure Appl. Geophys., 176, 4177-4211, doi:10.1007/s00024-019-02154-y.

Ganas, A., I. Oikonomou and C. Tsimi (2013). NOAfaults: A digital database for active faults in Greece, B. Geol. Soc. Greece, 47, 518-530, doi:10.12681/bgsg.11079.

Gönenç, T. (2021). Availability of TOPEX V28. 1 gravity data across the continent excluding seas; A case study, Western Anatolia example, Pamukkale Univ. J. Eng. Sci., 27, 6, doi:10.5505/pajes.2020.32654.

Hatzfeld, D., V. Karakostas, M. Ziazia, G. Selvaggi et al. (1997). The Kozani-Grevena (Greece) earthquake of 13 May 1995 revisited from a detailed seismological study, Bull. Seismol. Soc. Am., 87, 2, 463-473, doi:10.1785/BSSA0870020463.

Hatzfeld, D., D. Kementzetzidou, V. Karakostas, M. Ziazia et al. (1996). The Galaxidi earthquake of 18 November 1992: A possible asperity within the normal fault system of the Gulf of Corinth (Greece), Bull. Seismol. Soc. Am., 86, 6, 1987-1991, doi:10.1785/BSSA0860061987.

Hatzfeld, D., G. Pedotti, P. Hatzidimitriou, D. Panagiotopoulos et al. (1989). The Hellenic subduction beneath the Peloponnesus: first results of a microearthquake study, Earth Planet. Sci. Lett., 93, 2, 283-291, doi:10.1016/0012-821X(89)90076-9.

Heidarzadeh, M., O. Necmioglu, T. Ishibe and A. C. Yalciner (2017). Bodrum-Kos (Turkey-Greece) Mw 6.6 earthquake and tsunami of 20 July 2017: a test for the Mediterranean tsunami warning system, Geosci. Lett., 4, 1, 1-11, doi:10.1186/s40562-017-0097-0.

Hodgson, J. H. and J. I. Cock (1957). Direction of faulting in the Greek earthquakes of August 9-13, 1953, Publications of the Dominion Observatory, Ottawa, 18, 22, Canada Department of Mines and Technical Surveys, doi:10.4095/314509.

Hsu, S.-K., J.-C. Sibuet and C.-T. Shyu (1996). High-resolution detection of geologic boundaries from potential-field anomalies: An enhanced analytic signal technique, Geophysics, 61, 2, 315-621, doi:10.1190/1.1443966.

Hu, G., W. Feng, Y. Wang, L. Li et al. (2022). Source characteristics and exacerbated tsunami hazard of the 2020 Mw 6.9 Samos earthquake in eastern Aegean Sea, J. Geophys. Res. Solid Earth, 127, 5, doi:10.1029/2022JB023961.

Jackson, J., J. Haines and W. Holt (1994). A comparison of satellite laser ranging and seismicity data in the Aegean region, Geophys. Res. Lett., 21, 25, 2849-2852, doi:10.1029/94GL02734.

Jackson, J. and D. McKenzie (1988). Rates of active deformation in the Aegean Sea and surrounding regions, Basin Res., 1, 3, 121-128, doi:10.1111/j.1365-2117.1988.tb00009.x.

Kahveci, M., A. Çırmık, F. Doğru, O. Pamukçu et al. (2019). Subdividing the tectonic elements of Aegean and Eastern Mediterranean with gravity and GPS data, Acta Geophys., 67, 491-500, doi:10.1007/s11600-019-00270-w.

Karakostas, V., M. Ilieva, A. Kostoglou, D. Tondaś et al. (2022). The 2017 Kos sequence: Aftershocks relocation and coseismic rupture process constrained from joint inversion of seismological and geodetic observations, Tectonophysics, 833, 229352, doi:10.1016/j.tecto.2022.229352.

Karakostas, V., O. Tan, A. Kostoglou, E. Papadimitriou et al. (2021). Seismotectonic implications of the 2020 Samos, Greece, Mw 7.0 mainshock based on high-resolution aftershock relocation and source slip model, Acta Geophys., 69, 3, 979-996, doi:10.1007/s11600-021-00637-y.

Karasözen, E., E. Nissen, P. Büyükakpınar, M. D. Cambaz et al. (2018). The 2017 July 20 M w 6.6 Bodrum-Kos earthquake illuminates active faulting in the Gulf of Gökova, SW Turkey, Geophys. J. Int., 214, 1, 185-199, doi:10.1093/gji/ggy114.

Karkani, A., N. Evelpidou, M. Tzouxanioti, A. Petropoulos et al. (2021). Tsunamis in the Greek region: an overview of geological and geomorphological evidence, Geosciences, 12, 1, 4, doi:10.3390/geosciences12010004.

Kiratzi, A. A. (2014). Mechanisms of Earthquakes in Aegean. In: Beer, M., I. Kougioumtzoglou, E. Patelli, I.K. Au (eds) Encyclopedia of Earthquake Engineering. Springer, Berlin, Heidelberg. doi:10.1007/978-3-642-36197-5_299-1.

Kiratzi, A., C. Papazachos, A. Özacar, A. Pinar et al. (2021). Characteristics of the 2020 Samos earthquake (Aegean Sea) using seismic data, Bull. Earthquake Eng., 20, 7713-7735, doi:10.1007/s10518-021-01239-1.

Kiratzi, A. A. and C. A. Langston (1989). Estimation of earthquake source parameters of the May 4, 1972 event of the Hellenic arc by the inversion of waveform data, Phys. Earth Planet. Inter., 57, 3-4, 225-232, doi:10.1016/0031-9201(89)90113-1.

Kiratzi, A. A. and C. A. Langston (1991). Moment tensor inversion of the 1983 January 17 Kefallinia event of Ionian islands (Greece), Geophys. J. Int., 105, 2, 529-535, doi:10.1111/j.1365-246X.1991.tb06731.x.

Kiratzi, A. A., G. S. Wagner and C. A. Langston (1991). Source parameters of some large earthquakes in Northern Aegean determined by body waveform inversion, Pure Appl. Geophys., 135, 515-527, doi:10.1007/BF01772403.

Kkallas, C., C. Papazachos, E. Scordilis and B. Margaris (2013). Re-examining the stress field of the broader southern Aegean subduction area using an updated focal mechanism database, Bul. Geol. Soc. Greece, 47, 2, 563-573, doi:10.12681/bgsg.11083.

Konca, A. O., S. E. Guvercin, S. Ozarpaci, A. Ozdemir et al. (2019). Slip distribution of the 2017 M w6. 6 Bodrum-Kos earthquake: resolving the ambiguity of fault geometry, Geophys. J. Int., 219, 2, 911-923, doi:10.1093/gji/ggz332.

Kuleli, S. H. (1997). Seismicity and tectonics of the Aegean region, Bulletin of the International Institute of Seismology and Earthquake Engineering, 31, 391-405.

Le Pichon, X. (1983). Land-locked oceanic basins and continental collision: the Eastern Mediterranean as a case example, In: Mountain building processes, 201-211.

Le Pichon, X. and J. Angelier (1979). The Hellenic arc and trench system: a key to the neotectonic evolution of the eastern Mediterranean area, Tectonophysics, 60, 1-2, 1-42, doi:10.1016/0040-1951(79)90131-8.

Le Pichon, X. and J. Angelier (1981). The Aegean Sea, Philos. Trans. R. Soc. Lond. A Math. Phys. Sci., 300, 1454, 357-372, doi:10.1098/rsta.1981.0069.

Li, L., G. Ma and X. Du (2013). Edge detection in potential-field data by enhanced mathematical morphology filter, Pure Appl. Geophys., 170, 645-653, doi:10.1007/s00024-012-0545-x.

Main, I. G. and P. W. Burton (1989). Seismotectonics and the earthquake frequency-magnitude distribution in the Aegean area, Geophys. J. Int., 98, 3, 575-586, doi:10.1111/j.1365-246X.1989.tb02291.x.

McClusky, S., S. Balassanian, A. Barka, C. Demir et al. (2000). Global Positioning System constraints on plate kinematics and dynamics in the eastern Mediterranean and Caucasus, J. Geophys. Res. Solid Earth, 105, B3, 5695-5719, doi:10.1029/1996JB900351.

McClusky, S., R. Reilinger, S. Mahmoud, D. Ben Sari et al. (2003). GPS constraints on Africa (Nubia) and Arabia plate motions, Geophys. J. Int., 155, 1, 126-138, doi:10.1046/j.1365-246X.2003.02023.x.

McKenzie, D. (1972). Active tectonics of the Mediterranean region, Geophys. J. Int., 30, 2, 109-185, doi:10.1111/j.1365-246X.1972.tb02351.x.

McKenzie, D. P. (1978). Active tectonics of the Alpine-Himalayan belt: the Aegean Sea and surrounding regions, Geophys. J. Int., 55, 1, 217-254, doi:10.1111/j.1365-246X.1978.tb04759.x.

McKenzie, D. P. (1970). Plate tectonics of the Mediterranean region, Nature, 226, 5242, 239-243, doi:10.1038/226239a0.

Mercier, J., D. Sorel, P. Vergely, and K. Simeakis (1989). Extensional tectonic regimes in the Aegean basins during the Cenozoic, Basin Res., 2, 1, 49-71, doi:10.3390/w13162267.

Miller, H. G. and V. Singh (1994). Potential field tilt – a new concept for location of potential field sources, J. Appl. Geophys., 32, 2-3, 213-217, doi:10.1016/0926-9851(94)90022-1.

Moshou, A. (2020). Strong Earthquake Sequences in Greece during 2008-2014: Moment Tensor Inversions and Fault Plane Discrimination, Open J. Earthq. Res., 9, 04, 323-348, doi:10.4236/ojer.2020.94019.

Nasuti, Y. and A. Nasuti (2018). NTilt as an improved enhanced tilt derivative filter for edge detection of potential field anomalies, Geophys. J. Int., 214, 1, 36-45, doi:10.1093/gji/ggy117.

Oksum, E., D. Le, M. Vu, T. Nguyen et al. (2021). A novel approach based on the fast sigmoid function for interpretation of potential field data, Bull. Geophys. Oceanogr., 62, 3, 543-556, doi:10.4430/bgta0348.

Oral, B. M., R. E. Reilinger, M. Nafi Toksöz, R. W. King et al. (1995). Global positioning system offers evidence of plate motions in eastern Mediterranean, Eos Trans. Am. Geophys. Union, 76, 2, 9-11, doi:10.1029/EO076i002p00009-01.

Över, S., S. Özden, E. K. Ertan, F. Turhan et al. (2021). The 20 July 2017 Bodrum-Kos Earthquake (Mw 6.6) in southwestern Anatolia, Turkey, Earth Sci. Res. J., 25, 3, 309-321, doi:10.15446/esrj.v25n3.87080.

Öztürk, S. and Ş. Şahin (2019). A statistical space-time-magnitude analysis on the aftershocks occurrence of the July 21th, 2017 Mw = 6.5 Bodrum-Kos, Turkey, earthquake, J. Asian Earth Sci., 172, 443-457, doi:10.1016/j.jseaes.2018.10.008.

Papadimitriou, E. (1993). Focal mechanism along the convex side of the Hellenic Arc, B. Geofis. Teor. Appl., 35, 140, 401-426.

Papadopoulos, G., A. Agalos, M. Charalampakis, C. Kontoes et al. (2019). Fault models for the Bodrum-Kos tsunamigenic earthquake (Mw 6. 6) of 20 July 2017 in the east Aegean Sea, J. Geodyn., 131, 101646, doi:10.1016/j.jog.2019.101646.

Papadopoulos, G. and B. Chalkis (1984). Tsunamis observed in Greece and the surrounding area from antiquity up to the present times, Mar. Geol., 56, 1-4, 309-317, doi:10.1016/0025-3227(84)90022-7.

Papadopoulos, G., D. Kondopoulou, G.-A. Leventakis and S. Pavlides (1986). Seismotectonics of the Aegean region, Tectonophysics, 124, 1-2, 67-84, doi:10.1016/0040-1951(86)90138-1.

Papadopoulos, G. A., E. Gràcia, R. Urgeles, V. Sallares et al. (2014). Historical and pre-historical tsunamis in the Mediterranean and its connected seas: Geological signatures, generation mechanisms and coastal impacts, Mar. Geol., 354, 81-109, doi:10.1016/j.margeo.2014.04.014.

Papathanassiou, G., S. Valkaniotis and S. Pavlides (2019). The July 20, 2017 Bodrum-Kos, Aegean Sea Mw = 6.6 earthquake; preliminary field observations and image-based survey on a lateral spreading site, Soil Dynam. Earthquake Eng., 116, 668-680, doi:10.1016/j.soildyn.2018.10.038.

Papazachos, B. (1961). A contribution to the research on the focal mechanism of earthquakes in Greece. Phd, Athens University, Greece.

Papazachos, B., E. Papadimitriou, A. Kiratzi, C. Papazachos et al. (1998). Fault plane solutions in the Aegean Sea and the surrounding area and their tectonic implication, Boll. Geof. Teor. Appl, 39, 3, 199-218.

Papazachos, C. (1999). Seismological and GPS evidence for the Aegean-Anatolia interaction, Geophys. Res. Lett., 26, 17, 2653-2656, doi:10.1029/1999GL900411.

Paradisopoulou, P. M., V. G. Karakostas, E. E. Papadimitriou, M. D. Tranos et al. (2006). Microearthquake study of the broader Thessaloniki area (Northern Greece), Ann. Geophys., 49, 4-5, doi:10.4401/ag-3112.

Putri, D., M. Nanda, S. Rizal, R. Idroes et al. (2019). Interpretation of gravity satellite data to delineate structural features connected to geothermal resources at Bur Ni Geureudong geothermal field, In: IOP Conf. Ser. Earth Environ. Sci., doi:10.1088/1755-1315/364/1/012003.

Reilinger, R., S. McClusky, D. Paradissis, S. Ergintav et al. (2010). Geodetic constraints on the tectonic evolution of the Aegean region and strain accumulation along the Hellenic subduction zone, Tectonophysics, 488, 1-4, 22-30, doi:10.1016/j.tecto.2009.05.027.

Reilinger, R., S. McClusky, P. Vernant, S. Lawrence et al. (2006). GPS constraints on continental deformation in the Africa-Arabia-Eurasia continental collision zone and implications for the dynamics of plate interactions, J. Geophys. Res. Solid Earth, 111,B5, doi:10.1029/2005JB004051.

Ritsema, A. R. (1974). The earthquake mechanisms of the Balkan region, Koninklijk Nederlands Meteorologisch Instituut, 1-36.

Roumelioti, Z., A. Kiratzi and C. Benetatos (2011). Time-Domain Moment Tensors for shallow (h ≤ 40 km) earthquakes in the broader Aegean Sea for the years 2006 and 2007: The database of the Aristotle University of Thessaloniki, J. Geodyn., 51, 2-3, 179-189, doi:10.1016/j.jog.2010.01.011.

Sandwell, D., E. Garcia, K. Soofi, P. Wessel et al. (2013). Toward 1-mGal accuracy in global marine gravity from CryoSat-2, Envisat, and Jason-1, Lead. Edge, 32, 8, 892-899, doi:10.1190/tle32080892.1.

Sandwell, D. T., R. D. Müller, W. H. Smith, E. Garcia et al. (2014). New global marine gravity model from CryoSat-2 and Jason-1 reveals buried tectonic structure, Science, 346, 6205, 65-67, doi:10.1126/science.1258213.

Sandwell, D. T. and W. H. Smith (2009). Global marine gravity from retracked Geosat and ERS-1 altimetry: Ridge segmentation versus spreading rate, J. Geophys. Res. Solid Earth, 114,B01411, doi:10.1029/2008JB006008.

Sboras, S., I. Lazos, S. Bitharis, C. Pikridas et al. (2021). Source modelling and stress transfer scenarios of the October 30, 2020 Samos earthquake: Seismotectonic implications, Turk. J. Earth Sci., 30, 8, 699-717, doi:10.3906/yer-2107-25.

Sboras, S., I. Lazos, E. Mouzakiotis, V. Karastathis et al. (2020). Fault modelling, seismic sequence evolution and stress transfer scenarios for the July 20, 2017 (Mw 6.6) Kos-Gökova Gulf earthquake, SE Aegean, Acta Geophys., 68, 1245-1261, doi:10.1007/s11600-020-00471-8.

Seyitoğlu, G. and B. C. Scott (1996). The cause of NS extensional tectonics in western Turkey: tectonic escape vs back-arc spreading vs orogenic collapse, J. Geodyn., 22, 1-2, 145-153, doi:10.1016/0264-3707(96)00004-X.

Smith, W. H. and D. T. Sandwell (1997). Global sea floor topography from satellite altimetry and ship depth soundings, Science, 277, 5334, 1956-1962, doi:10.1126/science.277.5334.1956.

Sorel, D., J.-L. Mercier, B. Keraudren and M. Cushing (1988). Le rôle de la traction de la lithosphère subductée dans l'évolution géodynamique plio-pléistocène de l'arc égéen: mouvements verticaux alternés et variations du régime tectonique, C. R. Acad. Sci. II, 307, 19, 1981-1986.

Sternai, P., L. Jolivet, A. Menant, and T. Gerya (2014). Driving the upper plate surface deformation by slab rollback and mantle flow, Earth Planet. Sci. Lett., 405, 110-118, doi:10.1016/j.epsl.2014.08.023.

Stucchi, M., A. Rovida, A. Gomez Capera, P. Alexandre et al. (2013). The SHARE European earthquake catalogue (SHEEC) 1000-1899, J. Seismol., 17, 523-544, doi:10.1007/s10950-012-9335-2.

Sun, Y.-S., S. Melgar, A. Ruiz-Angulo, A. Ganas et al. (2024). The 2020 M w 7.0 Samos (Eastern Aegean Sea) Earthquake: joint source inversion of multitype data, and tsunami modelling, Geophys. J. Int., 237, 3, 1285-1300, doi:10.1093/gji/ggae082.

Sun, Y., W. Yang, X. Zeng and Z. Zhang (2016). Edge enhancement of potential field data using spectral moments, Geophysics, 81, 1, G1-G11, doi:10.1190/geo2014-0430.1.

Tan, O. (2013). The dense micro-earthquake activity at the boundary between the Anatolian and South Aegean microplates, J. Geodyn., 65, 199-217, doi:10.1016/j.jog.2012.05.005.

Tan, O., E. E. Papadimitriou, Z. Pabucçu, V. Karakostas et al. (2014). A detailed analysis of microseismicity in Samos and Kusadasi (Eastern Aegean Sea) areas, Acta Geophys., 62, 1283-1309, doi:10.2478/s11600-013-0194-1.

Taymaz, T., J. Jackson and D. McKenzie (1991). Active tectonics of the north and central Aegean Sea, Geophys. J. Int., 106, 2, 433-490, doi:10.1111/j.1365-246X.1991.tb03906.x.

Taymaz, T., J. Jackson and R. Westaway (1990). Earthquake mechanisms in the Hellenic Trench near Crete, Geophys. J. Int., 102, 3, 695-731, doi:10.1111/j.1365-246X.1990.tb04590.x.

Taymaz, T., S. Yolsal-Çevikbilen, T. S. Irmak, F. Vera et al. (2022). Kinematics of the 30 October 2020 Mw 7.0 Néon Karlovásion (Samos) earthquake in the Eastern Aegean Sea: Implications on source characteristics and dynamic rupture simulations, Tectonophysics, 826, 229223, doi:10.1016/j.tecto.2022.229223.

Tepe, Ç. and H. Sözbilir (2017). Tectonic geomorphology of the Kemalpaşa Basin and surrounding horsts, southwestern part of the Gediz Graben, Western Anatolia, Geodin. Acta, 29, 1, 70-90, doi:10.1080/09853111.2017.1317191.

Tiryakioğlu, İ., B. Aktuğ, C. Yiğit, H. Yavaşoğlu et al. (2018). Slip distribution and source parameters of the 20 July 2017 Bodrum-Kos earthquake (Mw 6.6) from GPS observations, Geodin. Acta, 30, 1, 1-14, doi:10.1080/09853111.2017.1408264.

Triantafyllou, I. and G. A. Papadopoulos (2024). New Observational Material about Seismic and Non-Seismic Tsunamis in Greece and Surrounding Areas from 1900 to 2023, GeoHazards, 5, 1, 233-254, doi:10.3390/geohazards5010012.

Triantafyllou, I., F. Zaniboni, A. Armigliato, S. Tinti et al. (2020). The Large Earthquake (~M7) and Its Associated Tsunami of 8 November 1905 in Mt. Athos, Northern Greece, Pure Appl. Geophys., 177, 1267-1293, doi:10.1007/s00024-019-02363-5.

Vamvakaris, D., C. Papazachos, C. A. Papaioannou, E. Scordilis et al. (2016). A detailed seismic zonation model for shallow earthquakes in the broader Aegean area, Nat. Hazards Earth Syst. Sci., 16, 1, 55-84, doi:10.5194/nhess-16-55-2016, 2016.

Wessel, P., J. F. Luis, L. Uieda, R. Scharroo et al. (2019). The generic mapping tools version 6, Geochem. Geophys. Geosyst., 20, 11, 5556-5564.

Wiemer, S. (2001). A Software Package to Analyze Seismicity: ZMAP, Seismol. Res. Lett., 72, 3, 373-382, doi:10.1785/gssrl.72.3.373.

Wijns, C., C. Perez and P. Kowalczyk (2005). Theta map: Edge detection in magnetic data, Geophysics, 70, 4, L39-L43, doi:/10.1190/1.1988184.

Zelenin, E., D. Bachmanov, S. Garipova, V. Trifonov et al. (2021). The database of the active faults of Eurasia (AFEAD): Ontology and design behind the continental-scale dataset, Earth Syst. Sci. Data Discuss., 2021, 1-20, doi:10.5194/essd-2021-312.

***CORRESPONDING AUTHOR: Burcin DIDEM TAMTAS**,
Istanbul University-Cerrahpasa, Faculty of Engineering, Department of Geophysical Engineering,
Buyukcekmece Campus, Istanbul, Turkey
e-mail: burcin.tamtas@iuc.edu.tr